The Indonesian Biomedical Journal, Vol.18, No.5, October 2026, p.416-519 Print ISSN: 2085-3297, Online ISSN: 2355-9179

RESEARCH ARTICLE

Methotrexate-associated Zinc Oxide Nanoparticles Reduce Cell Viability and Alters *TP53* and *COX-2* Gene Expressions in MCF7 Breast Cancer Cells

Ali M. Ahmed[1,*], Israa Fawzi Hasan[2], Yazan A. Mahmood[3], Mustafa Adnan Zaidan[4]

[1]College of Medicine, Mustansiriyah University, Baghdad 10052, Iraq
[2]College of Biomedical Engineering, Department of Biomechanics, Baghdad 10071, Iraq
[3]Educational Rusafa Directorte II, Baghdad 10052, Iraq
[4]Medical Technical College, Al-Farahidi University, Baghdad 10069, Iraq

*Corresponding author. Email: ali.majeed@uomustansiriyah.edu.iq

Received date: Jul 22, 2026; Revised date: Sep 7, 2026; Accepted date: Sep 9, 2026

Abstract

BACKGROUND: Conventional breast cancer treatment faces a lot of challenges due to treatment resistance and undesirable side effects. Oxidative stress pathway is involved in the response of cancer cells to chemotherapeutic agents and nanomaterials, which is usually related to alteration of malondialdehyde (MDA), tumor protein p53 (TP53), and Cyclooxygenase-2 (COX-2). Methotrexate (MTX) has been proved to have anticancer effect, but its clinical use is limited. Associating it with zinc oxide (ZnO) could offer a means of enhancing the cellular effects of MTX. This study was conducted to synthesize MTX–ZnO nanoparticles (NPs) and evaluate their antiproliferative activity, oxidative stress, and *TP53* and *COX-2* gene expression in MCF7 breast cancer cells.

METHODS: MTX–ZnO NPs were synthesized and characterized using UV–Vis spectroscopy, dynamic light scattering, zeta potential analysis, scanning electron microscopy, and X-ray diffraction analysis. The MTT assay was used to evaluate the cytotoxic activity against MCF7 cells, enzyme-linked immunosorbent assay (ELISA) to evaluate MDA level, and quantitative real-time polymerase chain reaction (PCR) to evaluate *TP53* and *COX-2* expressions.

RESULTS: The synthesized MTX–ZnO NPs exhibited average hydrodynamic diameter of 56.8 nm, zeta potential of −21.9 mV, and predominantly spherical morphology. MTX–ZnO NPs showed a concentration dependent cytotoxicity, reducing MCF7 cell viability from 91% to 51%. Treatment with MTX–ZnO NPs resulted in increase of MDA levels (16.8 µM *vs.* 3.4 µM), suggesting the improvement of lipid peroxidation and oxidative stress after MTX–ZnO NPs treatment. In addition, *TP53* expression increased from approximately 1.5-fold to 10.5-fold and *COX-2* expression increased from approximately 3-fold to 57-fold.

CONCLUSION: MTX–ZnO NPs exhibited antiproliferative effects on MCF7 breast cancer cells and were associated with increased oxidative stress and upregulated *TP53* and *COX-2* expression. The results indicate the potential of MTX–ZnO NPs in breast cancer treatment researches.

KEYWORDS: methotrexate, zinc oxide nanoparticles, breast cancer, MCF7 cells, oxidative stress, TP53, COX-2

Indones Biomed J. 2026; 18(5): 429-37

Introduction

Breast cancer remains one of the leading causes of cancer-related death for women worldwide, despite advancements in its treatment. Current treatment options available for breast cancer therapy are chemotherapy, endocrine therapy, targeted therapy and radiotherapy; however these modalities face a lot of challenges due to resistance to treatment and its toxic side-effects.(1-3) Oxidative stress is associated with the molecular pathways involved in the response of cancer cells to chemotherapeutic agents and nanomaterials, and

Copyright © 2026 The Prodia Education and Research Institute.
This work is licensed under a Creative Commons Attribution-NonCommercial 4.0 International (CC-BY-NC) License.

in cell-cycle arrest, DNA repair, senescence and apoptosis of cancer cells. Oxidative stress is usually marked by the alteration of malondialdehyde (MDA). This pathway also involves tumor protein p53 (TP53), a tumor suppressor gene that may be regulated under oxidative stress, and Cyclooxygenase-2 (COX-2), which is associated with inflammatory and stress-related signaling pathways. TP53 and COX-2 both play a role in cellular stress response, but in different regulatory pathways.(4)

Methotrexate (MTX) is a chemotherapy and anti-metabolite agent used to treat several types of cancer by stopping cells from using folic acid to make and repair DNA. Though it has been proven to have anticancer effect, its clinical use is restricted due to its non-specific toxicity and limitations in drug delivery.(1-3) The zinc oxide (ZnO) nanoparticles (NPs) are considered as a promising carrier platform because of the surface functionality and biological properties. Therefore, the interaction of MTX and ZnO might enhance the interactions between MTX and cells compared to the free MTX. To understand the cellular response to MTX–ZnO NPs treatment, it is necessary to evaluate oxidative stress and cellular damage of the cancer cell.

MCF7 is a widely used breast cancer model cell line to assess the cellular response of cancer therapy. Several previous studies reported the effect of MTX–ZnO NPs on MCF7 cells, however the response of these cells to continuous 72 h exposure, and the relationship between the concentration-dependent cell viability, MDA levels, as well as *TP53* and *COX-2* gene expressions have not been fully characterized as of yet.(5,6) Thus, this study was to conducted to synthesize and characterize MTX–ZnO NPs and assess its concentration-dependent effects on the viability of the MCF7 cells, MDA levels, and *TP53* and *COX-2* expressions after 72 h exposure.

Methods

MTX–ZnO NPs Preparation

Carbodiimide mediated coupling procedure was used to prepare the MTX-associated ZnO NPs (further referred to MTX–ZnO NPs).(7) Briefly, a suspension of ZnO NPs was mixed with MTX in 4-(2-hydroxyethyl)-1-piperazineethanesulfonic acid (HEPES) buffer and then 1-ethyl-3-(3-dimethylaminopropyl) carbodiimide (EDC) was used as a coupling agent. The reaction mixture consisted of 800 µL of ZnO NP suspension, 50 mM HEPES buffer, 5 mM EDC and MTX at 3 mg/mL, which resulted in final volume of 1 mL. The reaction mixture was shaken gently at 30°C for 5 h for the MTX interaction with the surface of the ZnO NPs to take place.(8)

After the association process, MTX–ZnO NPs were centrifuged at 10,000 rpm for 10 min and washed several times with deionized water to remove the free drug molecules and reagents. The resulting MTX–ZnO NPs were then resuspended in sterile deionized water and kept at 4°C for further physicochemical characterization and biological evaluation.(9)

Physicochemical Characterization of MTX–ZnO NPs

The hydrodynamic size distribution of MTX–ZnO NPs was obtained by dynamic light scattering (DLS) and the zeta potential was investigated by electrophoretic light scattering using a Zetasizer Nano ZS instrument (Malvern Instruments Ltd., Malvern, UK).(10) Meanwhile, the optical properties of the synthesized MTX–ZnO NPs were evaluated by UV–visible (UV–Vis) spectroscopy and the changes in the spectra due to the incorporation of MTX were assessed. (11) A UV–Vis spectrophotometer was used to record the spectra in the range of 200–800 nm. The prepared MTX–ZnO NPs were analyzed by the X-ray diffraction (XRD) analysis, which was carried out in a 2θ scanning range of 10-80°. Morphological characteristics were studied using scanning electron microscopy (SEM) and Particle size was determined from SEM micrographs by measuring several representative particles from SEM micrograph image using image analysis software, Image J (National Institute of Health, Bethesda, MD, USA).(12)

Cell Culture

The human breast adenocarcinoma cells, MCF7 were purchased from American Type Culture Collection (ATCC, Manassas, VA, USA). Cells were cultured in Dulbecco's Modified Eagle Medium (DMEM) with 10% fetal bovine serum (FBS), 100 U/mL penicillin and 100 µg/mL streptomycin and were grown at 37°C in a humidified atmosphere with 5% CO_2 and were routinely subcultured to ensure exponential growth throughout the experiment.

Cytotoxicity by MTT Assay

MTT colorimetric assay was used to evaluate the cytotoxic effects of MTX and MTX–ZnO NPs against MCF7 cells.(14) The cells were seeded at 4 × 10^4 cells/mL into 96-well plates and allowed to attach overnight. After cell attachment, cells were treated with 50 ng/mL free MTX or MTX–ZnO NPs at various concentrations of 3.12, 6.25, 12.5, 25, 50 ng/mL and were cultured for 72 h. The sham

group was provided with the same vehicle without MTX and ZnO nanoparticles.

The culture medium was then replaced with MTT solution (2.5 mg/mL) following treatment.(15) Plates were again incubated for an additional 4 h in darkness at 37°C for the formation of formazan crystals in the cells. The MTT solution was then removed, and the formazan crystals were dissolved in dimethyl sulfoxide (DMSO). The absorbance value was determined at 492 nm with a microplate reader. The viability of cells was determined by the following formula (16): Cell Viability (%) = (Absorbance of treated cells / Absorbance of control cells) × 100. All experiments were repeated three times, and the results are expressed as a percentage of untreated control cells. After each treatment condition, the analysis was made in three replicate wells.

Determination of MDA Levels

After treatment, the cell lysates were prepared to assess the intracellular oxidative stress by measuring MDA levels, an accepted marker of lipid peroxidation.(16) The MDA concentration was detected using MDA (Malondialdehyde) ELISA Kit (Cat. No. E-EL-0060; Elabscience Biotechnology Inc, Wuhan, China) following the manufacturer's instruction.(17) The kit has detection range of 31.25-2000 ng/mL and sensitivity of 18.75 ng/mL. Absorbance was read on a microplate reader and the concentrations of MDA were determined on a standard calibration curve. All measurements were repeated three times.

RNA Isolation and Quantitative Real-Time Polymerase Chain Reaction (PCR)

Total RNA was isolated from cancer MCF7 cells and untreated MCF7 cells using TRIzol reagent, following manufacturer's instructions.(18) Before complementary DNA (cDNA) synthesis, the purity and concentration of the isolated RNA was determined spectrophotometrically. Total RNA was reverse transcribed with oligo (dT) primers and cDNA was obtained.(19) This was followed by the quantitative real-time PCR, which was carried out using the SyBR Green chemistry technique on an ABI StepOnePlus Real-Time PCR System (Applied Biosystems, Waltham, MA, USA).

The expression of each *TP53* and *COX-2* was normalised to glyceraldehyde 3-phosphate dehydrogenase (*GAPDH*) as a housekeeping gene.(20) The relative gene expression was determined with comparative threshold cycle ($2^{-\Delta\Delta Ct}$) method. All reactions were performed in triplicate. Primer sequences of *TP53*, *COX-2*, and *GAPDH* were listed in Table 1.

Statistical Analysis

Data were analyzed using GraphPad Prism software (GraphPad Software, La Jolla, CA, USA).(21) One-way analysis of variance (ANOVA) was employed and the Dunnett's post hoc test was used for the differences among experimental groups.(22) A $p<0.05$ was deemed statistically significant.

Results

Physicochemical Characterization of MTX–ZnO NPs

The nanoscale particles formed have relatively uniform particle size distribution, as shown by the DLS analysis (Figure 1A) with an average hydrodynamic diameter of 56.8 nm (Table 2). The electrostatic repulsion between the particles provides moderate colloidal stability and the zeta potential is measured as −21.9 mV (Figure 1B).

The characterization of MTX–ZnO NPs using UV–Vis absorption spectrum showed the characteristic absorption band at around 341 nm (Figure 1C) indicative of the optical properties of the prepared MTX–ZnO NPs. The XRD pattern of the prepared nanoparticles revealed the characteristic peaks of ZnO (Figure 1D), confirming the crystallinity of the synthesized nanoparticles. The diffraction peaks were found at around 31.7°, 34.4°, 36–38°, 47.5°, 56.5°, 62.8°, 66.3° and 72.5° which were in good agreement with the characteristic reflections of hexagonal wurtzite ZnO. The diffraction pattern obtained was consistent with the previously reported hexagonal wurtzite ZnO and no additional impurity peaks were observed.

The micrographs obtained by SEM showed predominantly spherical nanoparticles of size about 55 to 58 nm (Figure 1E). SEM analysis showed the average

Table 1. Sequences of primers used for quantitative real-time PCR.

Gene	Forward Primer (5–3)	Reverse Primer (5–3)
TP53	ACAGCGTGGTGGTACCGTAT	GGAGCTGTTGCACATGTACT
COX-2	AGCTTGTGTGTGAGTGGTAG	TGAGAGATGGGCTGTTGTGT
GAPDH	AAGTTCAACGGCACAGTCAAGG	CATACTCAGCACCAGCATCACC

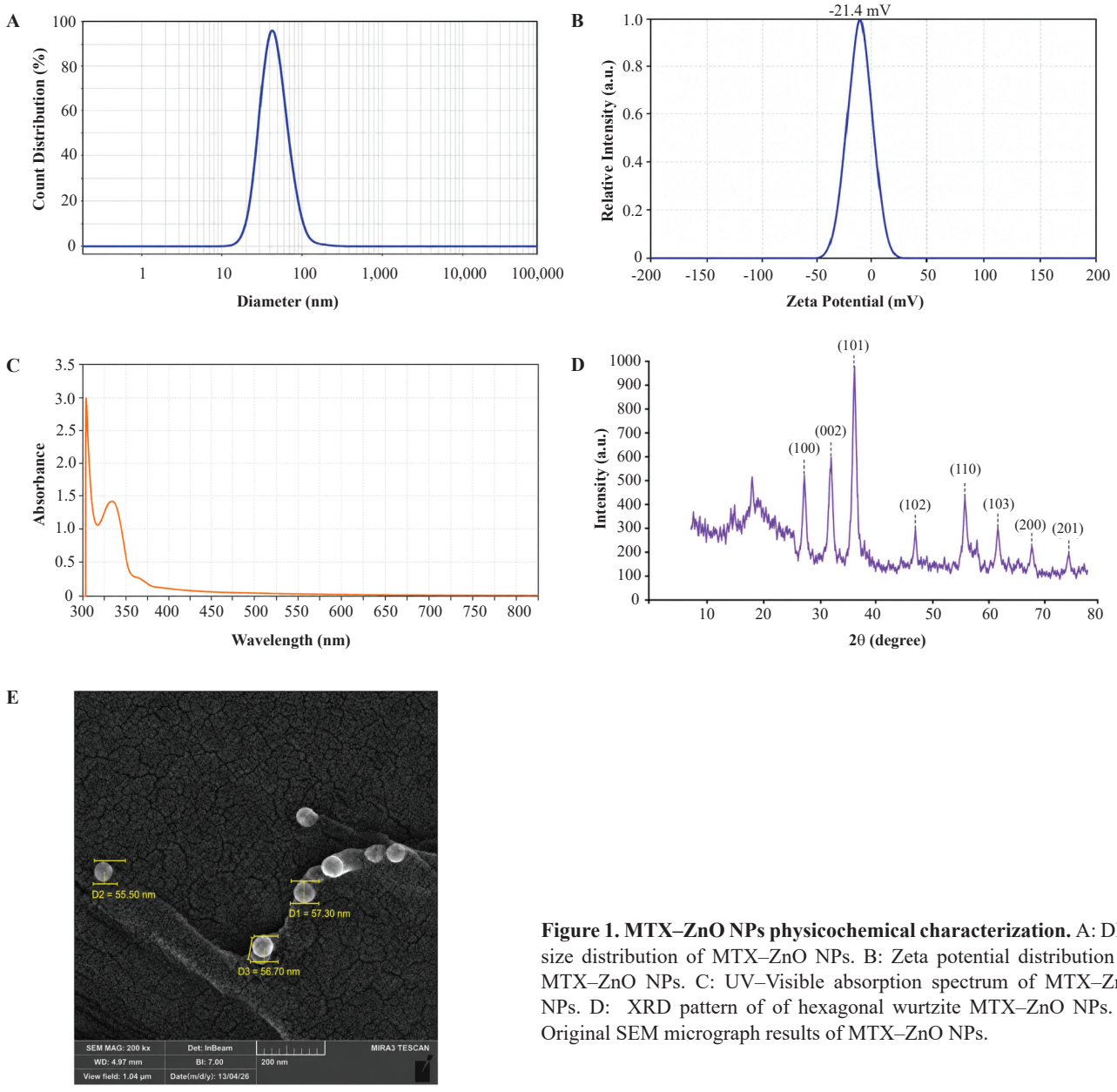


Figure 1. MTX–ZnO NPs physicochemical characterization. A: DLS size distribution of MTX–ZnO NPs. B: Zeta potential distribution of MTX–ZnO NPs. C: UV–Visible absorption spectrum of MTX–ZnO NPs. D: XRD pattern of of hexagonal wurtzite MTX–ZnO NPs. E: Original SEM micrograph results of MTX–ZnO NPs.

particle size of approximately 56.50 nm which was in good agreement with the hydrodynamic diameter obtained from DLS analysis, indicating the presence of relatively homogenous population of nanoparticles.

MTX–ZnO NPs Reduced MCF7 Cell Viability in a Concentration-dependent Manner

The effect of free MTX and MTX–ZnO NPs on the viability of MCF7 breast cancer cells after 72 h of treatment was assessed, and it was observed that the viability rate of MCF7 cells was close to 100% and was significantly higher than the viability rate of the sham treated cells (97%) in either case (p<0.05). Meanwhile, 50 ng/mL free MTX treatment led to cell viability of around 60% (Figure 2).

MTX–ZnO NPs caused a dose-dependent decrease in cell viability. Cell viability values were approximately 91%, 86%, 70%, 60%, and 51% following treatment with 3.12, 6.25, 12.5, 25, and 50 ng/mL MTX–ZnO NPs, respectively.

Table 2. Particle size measurements.

Measured Particle	Diameter (nm)
D1	57.30
D2	55.50
D3	56.70
Average	56.50

D1, D2 and D3 are three measurements of the diameter of individual nanoparticles taken from the SEM image.

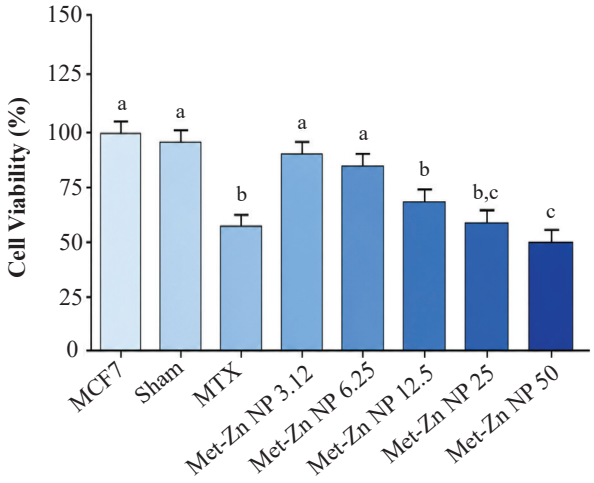


Figure 2. Viability of MCF7 cells after treatment for 72 h with MTX and MTX–ZnO NPs. Data are shown as mean±SD (n = 3). One-way ANOVA was carried out and Dunnett's test used for statistical analysis. Significant differences (p<0.05) are shown by different letters.

The results revealed that the viability of cells treated with MTX–ZnO NPs was comparable to the control group at concentrations of 3.12 and 6.25 ng/mL, while significant decreases were observed at 12.5 ng/mL and higher (p<0.05). Cells treated with 50 ng/mL of MTX–ZnO NPs had the lowest viability, significantly different from the low-dose and control groups. The results indicated that MTX–ZnO NPs showed a dose-dependent antiproliferative effect against the MCF7 breast cancer cells.

MTX–ZnO NPs Treatment Increased MDA Levels in MCF7 Cells

The low concentrations of MDA in the untreated cells and the sham-treated cells (approximately 3.4 µM and 3.0 µM, respectively) showed no significant difference between the two groups. The MDA was found to be significantly elevated with treatment of free MTX to about 12.0 µM. When treated with 50 ng/mL MTX–ZnO NPs, the increase was further observed with the concentration of MDA reaching about 16.8 µM (Figure 3).

From the results of the statistical analysis, it was concluded that there was significant difference between the MTX and MTX–ZnO NPs treatments and the untreated control group in terms of MDA. Furthermore, the group treated with MTX–ZnO NP had significantly higher MDA levels than the MTX treated group (p<0.05), indicating the lipid peroxidation was more significantly increased as a result of the drug delivery by ZnO NPs. These findings suggest that the increase in MDA accumulation might be a result of increased oxidative stress response in MCF7 cells when exposed to MTX–ZnO NPs than when treated with free MTX.

MTX–ZnO NPs Treatment Increased *TP53* Expression in MCF7 Cells

Cellular response to MTX and MTX–ZnO NPs treatment was evaluated by measuring the relative expression of *TP53* using real-time PCR. Low basal *TP53* levels (around 1.5-fold) were observed in both MCF7 cells and sham-treated cells and no difference was detected between these groups. Treatment with 50 ng/mL free MTX led to a significant up-regulation of *TP53* expression (~8.5-fold relative expression). In cells treated with 50 ng/mLMTX–ZnO NPs, a further increase was observed with expression of *TP53* reaching ~10.5-fold (Figure 4).

Two treatments of MTX and MTX–ZnO NPs were significantly different from the untreated and sham-treated groups in terms of *TP53* expression. Although the elevated expression of *TP53* was observed in the MTX–ZnO NP-treated group when compared to MTX-treated group, the difference between the two treatment groups was not statistically significant. The results suggest that free MTX and MTX–ZnO NPs may trigger *TP53*-associated cellular stress pathways with the highest *TP53* expression was observed in the MTX–ZnO NP group.

MTX–ZnO NPs Treatment Increased *COX-2* Expression in MCF7 Cells

To assess the effect of MTX and MTX–ZnO NPs treatment on the gene expression in MCF7 cells, the relative expression

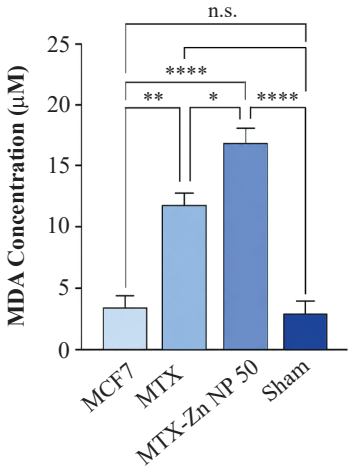


Figure 3. MDA levels in MCF7 cells after treatment with MTX and MTX–ZnO NPs. Data are shown as mean±SD (n = 3). One-way ANOVA and Dunnett's post hoc analysis was carried out. *p<0.05, **p<0.01, ****p<0.0001; n.s.: not significant.

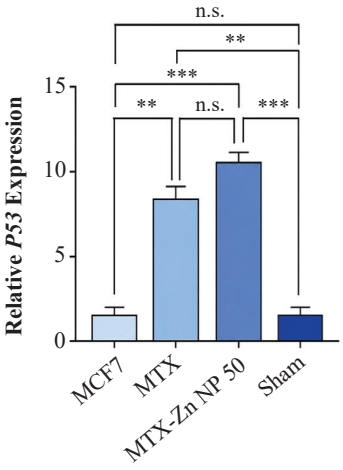


Figure 4. The relative *TP53* gene expression in the MCF7 cells treated with MTX and MTX–ZnO NPs. Data are shown as mean±SD (n = 3). One-way ANOVA and Dunnett's post hoc analysis was carried out. *p<0.05, **p<0.01, ***p<0.001; n.s.: not significant.

of *COX-2* was quantified. There was no significant difference between untreated MCF7 cells and sham-treated cells with the expression level of *COX-2* being similarly low in both cell groups. Treatment with 50 ng/mL free MTX significantly raised *COX-2* expression to ~ 36-fold relative expression. Cells treated with 50 ng/mL MTX–ZnO NPs showed an additional increase in the expression of *COX-2* as ~57-fold increase in relative expression (Figure 5).

The treated and untreated groups were found to be significantly different. MTX and MTX–ZnO NPs treatments significantly up-regulated the *COX-2* expression compared to the MCF7 and sham treated groups. *COX-2* expression was higher in the MTX–ZnO NP-treated group when compared to the MTX-treated group, but expression levels in both treatment groups were not statistically different. The highest *COX-2* expression was observed in the MTX–ZnO NPs experimental group.

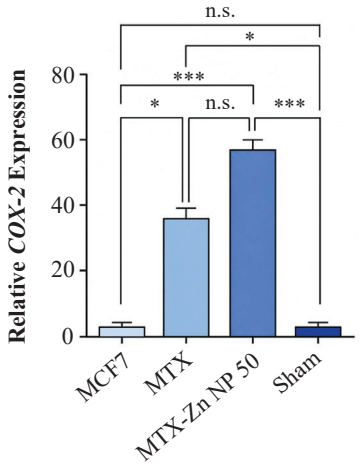


Figure 5. The relative *COX-2* gene expression in the MCF7 cells treated with MTX and MTX–ZnO NPs. Data are shown as mean±SD (n = 3). One-way ANOVA and Dunnett's post hoc analysis was carried out. *p<0.05, ***p<0.001; n.s.: not significant.

Discussion

NP-based drug delivery systems have emerged as promising systems to enhance the therapeutic activity of conventional anticancer drugs while reducing unwanted side effects in the systemic circulation.(23) MTX–ZnO NPs were successfully synthesized and characterized in the present study and the biological activity of NPs was investigated against MCF7 breast cancer cells.(24) The results showed that MTX–ZnO NPs had suitable physicochemical properties and were found to have concentration-dependent antiproliferative activity along with increased expression of *TP53* and *COX-2* and increased levels of oxidative stress.(25)

The physicochemical characterization of the prepared MTX–ZnO formulation showed its nanoscale properties.(26) Dynamic light scattering showed an average hydrodynamic diameter of 56.8 nm and SEM images indicated that the majority of nanoparticles were spherical, with an average size of about 56.50 nm. Results of the zeta potential of −21.9 mV showed that these particles had moderate colloidal stability, while the absorption band at about 341 nm in the UV-Vis spectra confirmed that the nanoparticles were being formed.(27) The results are in line with the previous reports on ZnO based nanocarriers as stable nanoscale materials which possess physicochemical properties suitable for biomedical applications.(28) In addition, the fairly uniform particle sizes found in the current study may facilitate nanoparticle–cell interactions.

The cytotoxicity results indicated that the MTX–ZnO NPs caused the decline of cell viability of MCF7 cells in a concentration-dependent manner.(29) The viability of the cells decreased gradually with increasing concentrations of the nanoparticles up to about 51% at the highest concentration used.(30) Cytotoxicity effects have also been observed, depending on the concentration of the nanomaterials, and are often explained by oxidative stress, impaired mitochondrial function and activation of cell death pathways in cancer cells. The antiproliferative effect is therefore congruent with the emerging data on the efficacy of the ZnO-based nanocarriers for anticancer applications.(31)

The increase in MDA levels after the MTX–ZnO NP treatment also highlights oxidative stress. MDA is regarded as a marker of lipid peroxidation and oxidative damage to

the cells.(32) The MDA level was significantly higher in cells treated with MTX–ZnO NP than in untreated and free methotrexate-treated cells, showing enhanced oxidative stress after MTX–ZnO NP treatment.(33) The observations are in line with other reports that ZnO nanoparticles cause oxidative stress and overproduction of reactive oxygen species (ROS), which results in cell damage.(34)

These gene expression data are also suggestive of mechanisms of cellular stress. The expression of *TP53* increased significantly after treatment with both free MTX and MTX–ZnO NPs with the highest expression observed in the MTX–ZnO NPs treated group.(35) *TP53* plays a critical role in regulating responses to DNA damage, cell-cycle arrest and apoptosis during cellular stress.(36) The expression of *TP53* was found to be higher in the MTX–ZnO NP-treated group but it was not found to be statistically significant when compared with the free MTX-treated group.(37) The simultaneous rise in *TP53* expression and MDA levels, however, as well as the drop in cell viability, were indicative of activation of stress pathways following NP treatment.

The expression of *COX-2* was also significantly elevated following treatment. *COX-2* is commonly associated with inflammatory signaling; however, it has been shown that it can be also induced by oxidative and cellular stress.(38) The expression of *COX-2* was found to be up-regulated in both free methotrexate and MTX–ZnO NP-treated groups when compared with untreated control group.(39) The *COX-2* expression was highest in the MTX–ZnO NP-treated group, but was not statistically different from free MTX.(40) The results indicate that the up-regulation of *COX-2* might be a stress response to MTX–ZnO NP treatment.

Exposure to MTX–ZnO NPs was associated with increased oxidative stress along with elevated expression of *TP53* and *COX-2*, and reduced viability of MCF7 cells. These findings support the antiproliferative activity of MTX–ZnO NPs and suggest an association between oxidative stress and their biological effects. Further studies are needed to elucidate the molecular mechanisms underlying the effect.

This study evaluated the effect of free MTX and MTX–ZnO NPs in various concentration, however, there is no control group of pure ZnO to allow the individual effect of ZnO on the MTX–ZnO system. This should be considered for future research to be included. There was also no specific procedures performed to determine whether there is interference in the MTT assay associated with the use of these nanoparticles. Additionally, chemical proof of MTX association and quantitative drug loading efficiency were not quantified. Protein-level assessment of TP53 and COX-2 and evaluation of additional inflammatory mediators such as nuclear factor-kappaB (NF-κB), tumor necrosis factrot (TNF)-α, and prostaglandin E2 (PGE2) were not performed and should be included in further studies. The observed increase in MDA and gene expression are associations with decreased cell viability and not direct evidence of cytotoxicity. Further assays looking at activation of pathways, apoptosis and ROS generation are needed to determine the mechanism. Finally, the results are presented in an *in vitro* model of MCF7 cells, so replication in other experimental models might be useful.

Conclusion

The MTX–ZnO NPs were successfully synthesized and characterized by nanoscale dimensions and favorable physicochemical properties. MTX–ZnO NPs exhibited concentration-dependent antiproliferative activity against MCF7 breast cancer cells accompanied by increased MDA levels; upregulated *TP53* and *COX-2* gene expressions were also observed. These results suggest that the antiproliferative effect of MTX–ZnO NPs might be associated with cellular stress responses in cells and also to a decrease in the viability of MCF7 cells. The results indicate the potential of MTX–ZnO NPs in breast cancer treatment researches.

Authors Contribution

AMA conceived and designed the research. AMA, IFH, and YAM contributed to data acquisition and analysis. AMA, IFH, YAM, and MAZ contributed to the interpretation of the results. AMA prepared the manuscript, while AMA and YAM designed the figures and tables. All authors contributed to the critical revision of the manuscript and approved the final version.

Ethical Statement

No human subjects or experimental animals were used in this study. Since the experiments were performed using the commercially available human breast cancer cell line MCF-7, MCF-7, that is commercially available, no ethical approval or informed consent was necessary.

Conflict of Interest

The authors declare that they have no conflict of interest.

References

1. Ju S, Singh MK, Han S, Ranbhise J, Ha J, Choe W, *et al.* Oxidative stress and cancer therapy: Controlling cancer cells using reactive oxygen species. Int J Mol Sci. 2024; 25(22): 12387. doi: 10.3390/ijms252212387.
2. Capuozzo M, Santorsola M, Bocchetti M, Perri F, Cascella M, Granata V, *et al.* p53: From fundamental biology to clinical applications in cancer. Biology. 2022; 11(9): 1325. doi: 10.3390/biology11091325.
3. Krishnamurthy HK, Pereira M, Rajavelu I, Jayaraman V, Krishna K, Wang T, *et al.* Oxidative stress: Fundamentals and advances in quantification techniques. Front Chem. 2024; 12: 1470458. doi: 10.3389/fchem.2024.1470458.
4. Kim JH, Dareowolabi BO, Thiruvengadam R, Moon EY. Application of nanotechnology and phytochemicals in anticancer therapy. Pharmaceutics. 2024; 16(9): 1169. doi: 10.3390/pharmaceutics16091169.
5. Ahmed AM, Shehab RM, Zaidan MA, Saadoon NM. Zinc oxide nanoparticles conjugated with methotrexate: Anti-proliferative impacts via P53 and COX-2 pathway control in MCF-7 breast cancer cells. J Nanostruct. 2026; 16(1): 353-64.
6. Bhattacharya S, Shinde RN, Beldar V, Khan R. Study of caspase-6 activity in aggressive HCT116 cells using methotrexate-encapsulated lactoferrin-conjugated solid lipid nanoparticles via in silico and in vitro approaches. Sci Rep. 2025; 15(1): 20775. doi: 10.1038/s41598-025-08089-w.
7. Mishra P, Ali Ahmad MF, Al-Keridis LA, Saeed M, Alshammari N, Alabdallah NM, *et al.* Methotrexate-conjugated zinc oxide nanoparticles exert a substantially improved cytotoxic effect on lung cancer cells by inducing apoptosis. Front Pharmacol. 2023; 14: 1194578. doi: 10.3389/fphar.2023.1194578.
8. Raut J, Sarkar O, Das T, Mandal SM, Chattopadhyay A, Sahoo P. Efficient delivery of methotrexate to MDA-MB-231 breast cancer cells by a pH-responsive ZnO nanocarrier. Sci Rep. 2023; 13(1): 21899. doi: 10.1038/s41598-023-49464-9.
9. Siddiqui AJ, Patel M, Adnan M, Jahan S, Saxena J, Alshahrani MM, *et al.* Bacteriocin-nanoconjugates (Bac10307-AgNPs) biosynthesized from Lactobacillus acidophilus-derived bacteriocins exhibit enhanced and promising biological activities. Pharmaceutics. 2023; 15(2): 403. doi: 10.3390/pharmaceutics15020403.
10. Elhabal SF, Abdelaal N, Saeed Al-Zuhairy SAK, Elrefai MFM, Elsaid Hamdan AM, Khalifa MM, *et al.* Green synthesis of zinc oxide nanoparticles from Althaea officinalis flower extract coated with chitosan for potential healing effects on diabetic wounds by inhibiting TNF-α and IL-6/IL-1β signaling pathways. Int J Nanomedicine. 2024; 19: 3045-70.
11. Joshi M, Bhatt P. Deciphering the anticancer activity of biocompatible zinc oxide nanoparticles loaded with methotrexate on breast cancer cells. Bull Mater Sci. 2023; 46(4): 192. doi: 10.1007/s12034-023-03044-9.
12. Nabi G, Ain QU, Tahir MB, Riaz KN, Iqbal T, Rafique M, *et al.* Green synthesis of TiO2 nanoparticles using lemon peel extract: their optical and photocatalytic properties. Int J Environ Anal Chem. 2022; 102(2): 434-42.
13. Prayogo AM, Wijaya AY, Hendrata WM, Looi SS, I'tishom R, Hakim L, *et al*. Dedifferentiation of MCF-7 breast cancer continuous cell line, development of breast cancer stem cells (BCSCs) enriched culture and biomarker analysis. Indones Biomed J. 2020; 12(2): 115-23.
14. Shariatifar H, Ranjbarian F, Hajiahmadi F, Farasat A. A comprehensive review on methotrexate containing nanoparticles; an appropriate tool for cancer treatment. Mol Biol Rep. 2022; 49(11): 11049-60.
15. Amirzadeh M, Soltanian S, Mohamadi N. Chemical composition, anticancer and antibacterial activity of Nepeta mahanensis essential oil. BMC Complement Med Ther. 2022; 22(1): 173. doi: 10.1186/s12906-022-03642-w.
16. Carmo de Carvalho e Martins M do, Martins AS da S, Oliveira LAS da S, Primo MG, Lira VBC. Biological indicators of oxidative stress [malondialdehyde, catalase, glutathione peroxidase, and superoxide dismutase] and their application in nutrition. In: Biomarkers in Nutrition. Cham: Springer International Publishing; 2022. p. 1-25.
17. Rotimi DE, Ojo OA, Adeyemi OS. Atrazine exposure caused oxidative stress in male rats and inhibited brain-pituitary-testicular functions. J Biochem Mol Toxicol. 2024; 38(1): e23579. doi: 10.1002/jbt.23579.
18. Al-Saeedi FJ. Asiaticoside increases caspase-9 activity in MCF-7 cells and inhibits TNF-α and IL-6 expression in nude mouse xenografts via the NF-κB pathway. Molecules. 2023; 28(5): 2101. doi: 10.3390/molecules28052101.
19. Tsiakanikas P, Adamopoulos PG, Tsirba D, Artemaki PI, Papadopoulos IN, Kontos CK, *et al*. High expression of a tRNAPro derivative associates with poor survival and independently predicts colorectal cancer recurrence. Biomedicines. 2022; 10(5): 1120. doi: 10.3390/biomedicines10051120.
20. da Conceição Braga L, Gonçalves BÔP, Coelho PL, da Silva Filho AL, Silva LM. Identification of best housekeeping genes for the normalization of RT-qPCR in human cell lines. Acta Histochem. 2022; 124(1): 151821. doi: 10.1016/j.acthis.2021.151821.
21. Cho H, Kwon HY, Sharma A, Lee SH, Liu X, Miyamoto N, *et al.* Visualizing inflammation with an M1 macrophage selective probe via GLUT1 as the gating target. Nat Commun. 2022; 13(1): 5974. doi: 10.1038/s41467-022-33526-z.
22. Macchi G, De Pisapia N. Virtual reality, face-to-face, and 2D video conferencing differently impact fatigue, creativity, flow, and decision-making in workplace dynamics. Sci Rep. 2024; 14(1): 10260. doi: 10.1038/s41598-024-60942-6.
23. Ahmed AM, Fadhil GA, Rahmah MI. Innovative use of commercial wipes as a template for the synthesis of ZnO and CuO nanoparticles via combustion method for antibacterial applications. Appl Nanosci. 2026; 16 (1): 10. doi: 10.1007/s13204-025-03142-6.
24. Ahmed AM, Mustafa MB, Kadhim DH, Zaidan MA, Shehab RM. Synthesis of silver nanoparticles by pulsed laser ablation: Structural, optical, in vitro antibacterial, and cytotoxicity properties. Indones Biomed J. 2026; 18(3): 213-22.
25. Ahmed AM, Shehab RM, Hammed MAN, Khalid GA, Jaber GS, Zaidan MA. Optimization of copper oxide nanoparticles production by pulsed laser ablation: A study on energy density effects. Ann Chim Sci Mater. 2025; 49(2): 157-62.
26. Zakinyan A, Ahmed AM, Kononenko D. Local field and deformation of droplets in emulsions. J Mol Liq. 2025; 427: 127406.
27. Ceballos-Chuc MC, Ramos-Castillo CM, Rodríguez-Pérez M, Ruiz-Gómez MÁ, Rodríguez-Gattorno G, Villanueva-Cab J. Synergistic correlation in the colloidal properties of TiO2 nanoparticles and its impact on the photocatalytic activity. Inorganics. 2022; 10(9): 125. doi: 10.3390/inorganics10090125.

28. Vagena IA, Gatou MA, Theocharous G, Pantelis P, Gazouli M, Pippa N, *et al.* Functionalized ZnO-based nanocomposites for diverse biological applications: Current trends and future perspectives. Nanomaterials. 2024; 14(5): 397. doi: 10.3390/nano14050397.
29. Negrescu AM, Killian MS, Raghu SNV, Schmuki P, Mazare A, Cimpean A. Metal oxide nanoparticles: Review of synthesis, characterization and biological effects. J Funct Biomater. 2022; 13(4): 274. doi: 10.3390/jfb13040274.
30. Kesharwani P, Halwai K, Jha SK, Al Mughram MH, Almujri SS, Almalki WH, *et al.* Folate-engineered chitosan nanoparticles: Next-generation anticancer nanocarriers. Mol Cancer. 2024; 23(1): 244. doi: 10.1186/s12943-024-02163-z.
31. Allam RM, El-Nasr NMEA, Elbaset MA, Saleh DO, El-Seidy AMA. Unveiling the potency of ZnO and CuO nanocomposites in combating hepatocellular carcinoma by inducing cell death and suppressing migration. Sci Rep. 2025; 15(1): 15477. doi: 10.1038/s41598-025-97395-4.
32. Alsemeh AE, Amin EE, Yassin HA, Eldousoky M, Mostafa W, AlShahat A. Evaluation of the protective effects of alpha-lipoic acid against zinc oxide nanoparticle-induced pulmonary injury in rats. Egypt Soc Clin Toxicol J. 2025; 13(1): 105-24.
33. Saleem MU, Muhammad F, Sharif A, Arshad MI, Akhtar K, Javed Y, *et al.* Methotrexate-loaded biodegradable nanoparticles exert anti-arthritic effect by downregulating pro-inflammatory cytokines in Freund's complete adjuvant-induced arthritic rats. Inflammopharmacology. 2022; 30(3): 1079-91.
34. Zhuo LB, Liu YM, Jiang Y, Yan Z. Zinc oxide nanoparticles induce acute lung injury via oxidative stress-mediated mitochondrial damage and NLRP3 inflammasome activation: In vitro and in vivo studies. Environ Pollut. 2024; 341: 122950. doi: 10.1016/j.envpol.2023.122950.
35. Hassan A, Al-Salmi FA, Abuamara TMM, Matar ER, Amer ME, Fayed EMM, *et al.* Ultrastructural analysis of zinc oxide nanospheres enhances anti-tumor efficacy against Hepatoma. Front Oncol. 2022; 12: 933750. doi: 10.3389/fonc.2022.933750.
36. Vaddavalli PL, Schumacher B. The p53 network: Cellular and systemic DNA damage responses in cancer and aging. Trends Genet. 2022; 38(6): 598-612.
37. Lestadi I, Siregar NC, Wuyung PE. The correlation between TP53 expression and Ki-67 proliferation with Bartl malignancy degree of plasma cell neoplasm. Indones Biomed J. 2017; 9(1): 35-42.
38. Khan H, Sharma K, Kumar A, Kaur A, Singh TG. Therapeutic implications of cyclooxygenase (COX) inhibitors in ischemic injury. Inflamm Res. 2022; 71(3): 277-92.
39. Kamal M, Mehta V, Rao M, Damerla RR, Pai A, Sharan K, *et al.* A mechanistic review of methotrexate and celecoxib as a potential metronomic chemotherapy for oral squamous cell carcinoma. Cancer Investig. 2023; 41(2): 144-54.
40. Hu J, Shi M, Tian M, Xie B, Tan Y, Zhou D, *et al.* Nanomedicine-driven therapeutic strategies for rheumatoid arthritis-associated depression: Mechanisms and pharmacological progress. Pharmaceuticals. 2026; 19(1): 94. doi: 10.3390/ph19010094.